Trapped electrons in vacuum for a scalable quantum processor

G. Ciaramicoli, I. Marzoli, and P. Tombesi
Dipartimento di Fisica and Unità INFM, Università degli Studi di Camerino, Camerino, Italy
(Received 5 May 2004; published 1 September 2004)

We describe in detail a theoretical scheme to trap and manipulate an arbitrary number of electrons in vacuum for universal quantum computation. The particles are confined in a linear array of Penning traps by means of a combination of static electric and magnetic fields. Two-electron operations are realized by controlling the Coulomb interaction between neighboring particles. The performances of such a device are evaluated in terms of clock speed, fidelity, and decoherence rates.

DOI: 10.1103/PhysRevA.70.032301 PACS number(s): 03.67.Lx, 03.67.Mn, 32.80.Pj

I. INTRODUCTION

In the search for the implementation of quantum computing, different schemes based on a variety of quantum systems have been proposed [1]. In the case of trapped ions, for example, there are already promising experimental demonstrations [2–5]. However, we are still at the proof-of-principle stage, where operations are limited to a small number of qubits. In the long run towards a winning technology for quantum computation, it is, hence, worthy to investigate new systems.

Our recent proposal [6] showed the possibility to realize a scalable quantum computer with trapped electrons in vacuum. This idea, extending previous schemes [7–9], has been encouraged by the impressive results obtained in the experiments with a single electron in a Penning trap [10–12] and by the recent advancements in three-dimensional (3D) microtrap costruction [13].

By using electrons in vacuum we combine the low-decoherence environment and experimental accuracy typical of ion traps [14,15] with the high clock speed, compactness, and scalability of solid-state devices [16,17]. In comparison with rf ion traps [14,15], we have, at least, three major advantages: (i) faster clock frequency of 2–3 orders of magnitude due to the smaller mass of the electron, (ii) weaker decoherence effects due to reduced field fluctuations, and (iii) dense coding with more qubits per site. Furthermore, with respect to solid-state proposals [16,17], vacuum traps for electrons minimize the environmental influence found in semiconductor devices and could create more accurate structures [13].

More specifically our system consists of a set of electrons confined in vacuum within an innovative trapping arrangement. Our scheme reproduces a linear array of Penning traps with interparticle distances ranging from 1.5 μm to 500 μm. Quantum information is encoded in the different quantized degrees of freedom of the electron motion as well as in the two states of the spin. The gate operations on single particles are performed by means of appropriate electromagnetic pulses. They permit, when combined with specific static inhomogeneous fields, one to achieve universal computation on the qubits of each single electron. In order to realize universal gates between qubits of different electrons we exploit the Coulomb interaction in the following way. Each trap confines a single electron which oscillates with its own axial frequency. When two neighboring particles are put into resonance, they may exchange a quantum of excitation [18]. If we are dealing with the lowest Fock states of the axial motion—i.e., $|0\rangle_z$ and $|1\rangle_z$—this operation amounts to a swapping gate. This ability, combined with the universal set of quantum gates on every single electron, allows us to implement conditional dynamics between different particles. The final qubit readout can be performed by either axial frequency detection, as in traditional Penning traps [10], or by capacitance and charge measurements, as in semiconductor quantum dots [19].

In this paper we present a detailed description and analysis of our system. In particular, we estimate its performances and efficiency when all the main error and decoherence sources are taken into account. The results of this investigation are very encouraging. They demonstrate that, in our scheme, error probabilities per gate less than 10^{-4} are within the reach of present technology. Hence, fault tolerant computation should be actually feasible.

The paper is organized as follows. We first describe the trapping structure (Sec. II), where the electrons are held. In Sec. III, we sketch how to implement universal computation with the qubits stored in each electron. In this section we also evaluate the fidelity of single-particle quantum gates. The following section, Sec. IV, is devoted to the analysis of the swapping gate between qubits of neighboring electrons. We describe this operation in detail and estimate its fidelity. This gate allows for two-particle universal operations, as shown in Sec. V. In Sec. VI we deal with the final qubit readout. The most relevant decoherence processes and their effects are analyzed in Sec. VII. Finally, we summarize our main results in Sec. VIII.

II. LINEAR ARRAY OF PENNING TRAPS

In this section we present a scheme for the implementation of a scalable quantum processor consisting of a linear array of electrons. Our aim is to confine the particles inside the same physical device, creating a periodic potential that locally well approximates the typical quadrupole potential, used in traditional Penning traps [20]. Ideally, each electron is confined to a small region, where the applied electrostatic potential plus a homogeneous magnetic field reproduce the usual field configuration of a Penning trap.

The device able to realize such a periodic confining structure consists of a cylindrical trap of radius r_0 and length z_0.

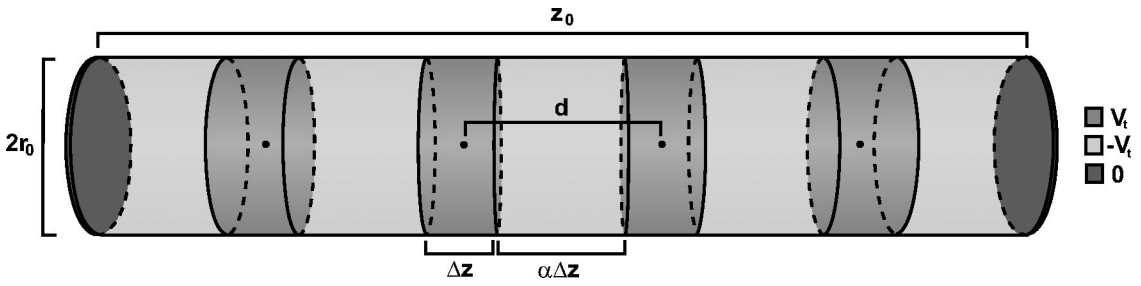

FIG. 1. Schematic drawing of a cylindrical trap with the lateral surface consisting of nine ring electrodes at alternate potentials. This device reproduces along the axial direction four Penning traps where electrons can be confined.

The bases of this cylinder are composed of flat electrodes at zero potential, whereas the lateral surface is made up by a set of N ring electrodes of width Δz_i, held at different potentials V_i and separated by thin dielectric layers. Note that no electrode is interposed between the electrons of the array, in order to prevent the electrostatic shielding.

The electrostatic potential inside this cavity can be analytically calculated [21,22]. To this end, we choose a set of cylindrical coordinates with the origin on the left basis of the cylinder and the z axis along the symmetry axis. With this choice, the potential inside the cylinder is given by the relation [21,22]

$$V(r,z) = \sum_{n=1}^{\infty} A_n \sin\left(\frac{n\pi z}{z_0}\right) \frac{I_0(n\pi r/z_0)}{I_0(n\pi r_0/z_0)}, \tag{1}$$

where the expansion coefficients are given by

$$\begin{aligned} A_n = \frac{4}{n\pi}\Bigg[& V_1 \sin^2\left(\frac{n\pi\Delta z_1}{2z_0}\right) \\ & + V_2 \sin\left(\frac{n\pi(\Delta z_2 + 2\Delta z_1)}{2z_0}\right)\sin\left(\frac{n\pi\Delta z_2}{2z_0}\right) \\ & + V_3 \sin\left(\frac{n\pi(\Delta z_3 + 2\Delta z_1 + 2\Delta z_2)}{2z_0}\right)\sin\left(\frac{n\pi\Delta z_3}{2z_0}\right) + \cdots \\ & + V_N \sin\left(\frac{n\pi(\Delta z_N + 2\Delta z_1 + 2\Delta z_2 + \cdots + 2\Delta z_{N-1})}{2z_0}\right) \\ & \times \sin\left(\frac{n\pi\Delta z_N}{2z_0}\right)\Bigg] \end{aligned} \tag{2}$$

and I_0 is the modified Bessel function of zero order. For particular values of the V_i's and the Δz_i's, the electrostatic potential energy of an electron inside the cavity presents, along the z axis, a series of minima where one can trap the particles. These are, actually, saddle points since the electrostatic potential provides only the confinement along the axial direction. To obtain the radial confinement as well, we have to introduce a homogeneous static magnetic field directed along the z axis. Thus, we can construct a kind of miniaturized Penning trap centered on each minimum. To obtain, for example, m minima we can choose the following configuration of trapping electrodes (see Fig. 1). We use $2m+1$ ring electrodes with potentials having alternate signs—i.e., $V_1 = -V_t$, $V_2 = +V_t$, $V_3 = -V_t, \ldots$, $V_{2m} = +V_t$, $V_{2m+1} = -V_t$. The electrode widths are $\Delta z_i = \alpha\Delta z$ for i odd and $\Delta z_i = \Delta z$ for i even with $\Delta z = z_0/[m+\alpha(m+1)]$ and $\alpha \geqslant 1$ so that the electrodes at the same potential have also the same width. In this case, the electrostatic potential energy of an electron has, along the z axis, minima located, to a good approximation, at the center of the positive electrodes (see Fig. 2)—that is, at the positions

$$z_1 = \left(\alpha + \frac{1}{2}\right)\Delta z, \quad z_2 = \left(2\alpha + \frac{3}{2}\right)\Delta z, \ldots,$$

$$z_m = \left(m\alpha + \frac{2m-1}{2}\right)\Delta z. \tag{3}$$

Electrons can be trapped around these equally spaced minima, separated by a distance $d = (\alpha+1)\Delta z$. In our design, the distance d between two neighboring particles ranges from 1.5 μm to 500 μm. To better study the form of the potential, Eq. (1), along the z axis we use an expansion with respect to a point $(0,\zeta)$:

$$\begin{aligned} V(r,z) &= \sum_{i=0}^{\infty} \mathcal{C}^{(i)}[r^2 + (z-\zeta)^2]^{i/2} P_i\left(\frac{z-\zeta}{\sqrt{(z-\zeta)^2 + r^2}}\right) \\ &= \mathcal{C}^{(0)} + \mathcal{C}^{(1)}(z-\zeta) + \mathcal{C}^{(2)}\left[(z-\zeta)^2 - \frac{r^2}{2}\right] \\ &\quad + \mathcal{C}^{(3)}\left[(z-\zeta)^3 - \frac{3}{2}(z-\zeta)r^2\right] \\ &\quad + \mathcal{C}^{(4)}\left[(z-\zeta)^4 - 3r^2(z-\zeta)^2 + \frac{3}{8}r^4\right] + \cdots, \end{aligned} \tag{4}$$

where

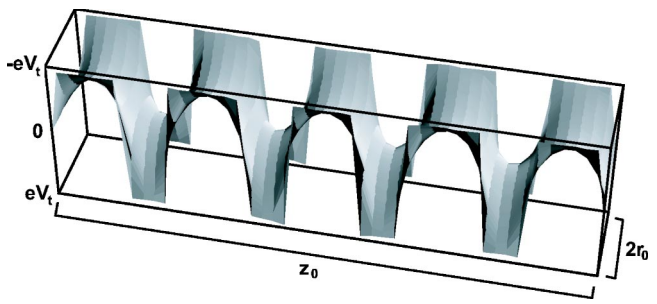

FIG. 2. Three-dimensional plot showing the electrostatic energy of the electron in the cylindrical trap sketched in Fig. 1. Electrons can be stored near the four minima along the z axis.

$$\mathcal{C}^{(i)} = \begin{cases} \dfrac{(-1)^{i/2}}{i!} \displaystyle\sum_{n=1}^{\infty} \dfrac{A_n}{I_0(n\pi r_0/z_0)} \left(\dfrac{n\pi}{z_0}\right)^i \sin\left(\dfrac{n\pi\zeta}{z_0}\right), & \text{for } i \text{ even}, \\ \dfrac{(-1)^{(i-1)/2}}{i!} \displaystyle\sum_{n=1}^{\infty} \dfrac{A_n}{I_0(n\pi r_0/z_0)} \left(\dfrac{n\pi}{z_0}\right)^i \cos\left(\dfrac{n\pi\zeta}{z_0}\right), & \text{for } i \text{ odd}. \end{cases} \tag{5}$$

and P_i is the Legendre polynomial of order i.

Near a minimum, the leading term in the expansion of the potential, Eq. (4), is the quadratic one, proportional to the coefficient $\mathcal{C}^{(2)}$. Hence, in a small region around the jth minimum z_j, we can approximate the electrostatic potential energy of an electron of charge e as

$$eV(r,z) \simeq e\mathcal{C}^{(2)}\left[(z-z_j)^2 - \frac{r^2}{2}\right], \tag{6}$$

where $\mathcal{C}^{(2)}$ is given by the expression (5) and $e\mathcal{C}^{(2)} > 0$. This relation represents a quadrupole potential which provides the axial confinement to the electron.

In this electrode arrangement energy minima not too close to the cylinder end caps have the following properties. The values of the coefficients $\mathcal{C}^{(i)}$ in the expansion (4) do not substantially depend on the minimum position. Furthermore, in the case of i odd, they are, in good approximation, negligible. These are consequences of the fact that, for minima located away from the trap end caps, the system is approximately symmetric with respect to a plane perpendicular to the z axis and containing the minimum. In this case we can write, for i even,

$$\mathcal{C}^{(i)} = \frac{V_t \overline{C}_t^{(i)}}{d^i}, \tag{7}$$

where the $\overline{C}_t^{(i)}$'s are dimensionless coefficients depending only on the geometrical properties of the system—i.e., the parameters r_0/d and α. Their values can be calculated from Eqs. (2) and (5).

Hence, from Eqs. (6) and (7), the axial oscillation frequency of the trapped electrons confined around these minima is

$$\omega_z \simeq \sqrt{\frac{2eV_t \overline{C}_t^{(2)}}{m_e d^2}}, \tag{8}$$

with m_e being the electron mass. This equation describes the dependence of the electron axial frequency on the trap size and on the potential applied to the ring electrodes. In our design the geometrical parameters r_0/d and α have ranges, respectively, of 0.2–0.5 and of 1–2.3, with $0.7 \lesssim (r_0/d)(1+\alpha) \lesssim 1$. This choice gives $\overline{C}_t^{(2)}$ in a range of -25 to -5 with the smallest values of $\overline{C}_t^{(2)}$ obtained for the smallest values of r_0/d and the largest values of α. Thus, with interparticle distances ranging from 500 μm to 1.5 μm we can easily produce trapping frequencies ranging from 3 MHz to 50 GHz by applying potential differences from 0.05 mV to 25 mV.

With the above geometrical parameters, at a distance d_m from the considered minimum not larger than $d/10$, the main correction to the quadrupole potential is given by the octupole term proportional to $\mathcal{C}^{(4)}$. Its size relative to the quadrupole term, obtained from Eq. (4), is of the order of $|\overline{C}_t^{(4)}/\overline{C}_t^{(2)}|(d_m/d)^2$ with $|\overline{C}_t^{(4)}/\overline{C}_t^{(2)}|$ in a range, according to the chosen geometry, 1–5.

The trapping electrodes permit one to create, together with the application of a uniform magnetic field in the axial direction, a linear array of Penning traps, each one having the same strength. However, as described in the next section, the implementation of quantum information processing requires a confining device with specific properties. First we want to control and vary in a suitable range the value of the octupole term of the trap potential. Second we want to manipulate the axial frequency of each electron without affecting the other trap parameters. Third we want to selectively apply to each trap an oscillating electric field. These tasks can be accomplished by adding to the cylindrical cavity three additional sets of electrodes.

The first one is composed, in a trap with m minima, by $2m$ ring electrodes, each one having width Δz_c with $\Delta z_c < \Delta z/2$ and held at potential V_c. These electrodes, called decompensating electrodes, permit, by varying V_c, to change the value of the octupole term in the trap potential. We need to increase the anharmonicity of the axial oscillator in order to manipulate the quantum information, encoded in the electron motion, without leaving the computational space. The anharmonic corrections make the transition frequencies of neighboring axial energy states distinguishable. Consequently, as discussed in the next section, an oscillating electric field with appropriate frequency can selectively act on specific axial transitions realizing single-qubit gates.

Two decompensating electrodes are inserted at the ends of each trapping electrode at potential V_t, as illustrated in Fig. 3(c). In practice, this addition requires the shortening of the positive trapping electrodes by a value of $2\Delta z_c$. Inside the cylindrical cavity the electrostatic potential $V(r,z)$ produced by this electrode arrangement can be written as

$$V(r,z) = V_T(r,z) + V_C(r,z). \tag{9}$$

In this relation $V_T(r,z)$ and $V_C(r,z)$ are the potentials obtained from Eq. (1) with, respectively, the trapping electrodes and the decompensating electrodes only. In particular, $V_C(r,z)$ is calculated with all the ring electrodes held at zero

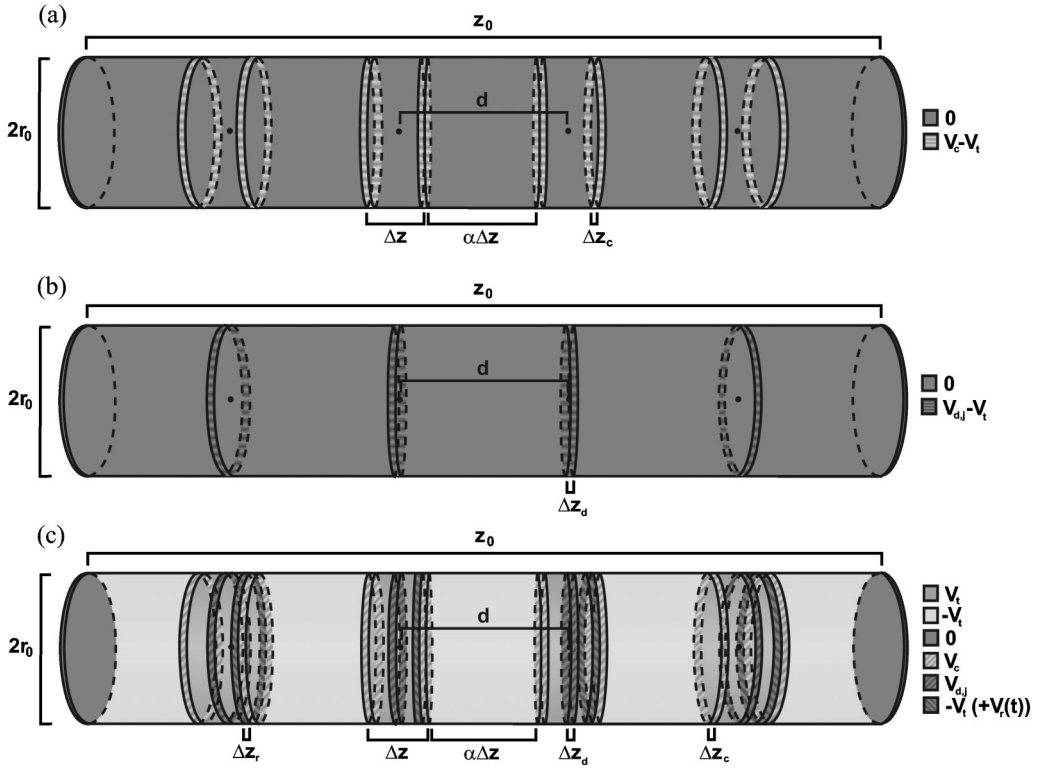

FIG. 3. Schemes (a) and (b) show the electrode arrangement giving, respectively, $V_C(r,z)$ and $V_D(r,z)$. Scheme (c) displays the complete trapping device with the lateral surface consisting of trapping, decompensating, detuning, and driving electrodes.

potential except the decompensating electrodes held at potential $V_c - V_t$ [see Fig. 3(a)].

Consequently the coefficients of the expansion (4) for a minimum not too close to the cylinder end caps can be written as

$$\mathcal{C}^{(i)} = \frac{V_t \overline{C}_t^{(i)}}{d^i} + \frac{(V_c - V_t)\overline{C}_c^{(i)}}{d^i}, \tag{10}$$

where the $\overline{C}_c^{(i)}$'s are dimensionless coefficients depending on the geometrical parameters r_0/d, α, and $\Delta z_c/\Delta z$. They can be obtained from Eq. (5). Again, we suppose that the $\overline{C}_c^{(i)}$'s do not depend on the minimum position and, for odd i, have negligible values.

Our aim is to increase the value of the octupole term of the trap potential by applying a not too large voltage V_c. At the same time, we also want to make the change on the trapping frequencies, produced by the potential of the decompensating electrodes, as small as possible. From Eq. (10) we see that these intents can be achieved by choosing a trap geometry which maximizes the ratio $|\overline{C}_c^{(4)}/\overline{C}_c^{(2)}|$. Indeed, for any couple of values of r_0/d and α it exists a particular value of the ratio $\Delta z_c/\Delta z$ which makes $\overline{C}_c^{(2)}$ equal to zero. This value, indicated by β_0, is, for our geometries, in the range 0.1–0.3. Hence, we can choose decompensating electrodes of length $\Delta z_c \simeq \beta_0 \Delta z$ in order to minimize their effect on the trap frequencies. Typical values are listed in Table I. In this case the corresponding values of the $|\overline{C}_c^{(4)}|$'s, depending on the parameter r_0/d and α, vary in a range 3–350, with the largest values obtained for the smallest and largest values of, respectively, r_0/d and α.

The second set of electrodes we add to our trapping device is composed, in the case of m minima, by m ring electrodes of equal width Δz_d with $\Delta z_d < \Delta z$. These electrodes, called detuning electrodes, are used to control and vary the axial trap frequencies. The selective manipulation of the trap frequencies is, in our scheme, a fundamental requirement. When the difference between the axial frequencies of two trapped electrons is sufficiently large, the particles substantially do not interact. On the other hand, the interaction is effective when the frequencies are on resonance. Generally we do not want interactions among all the trapped particles so we need to differentiate their axial frequencies. At the same time we should be able to put on and off resonance the frequencies of two neighboring electrons in order to control the interaction between them.

Each detuning electrode is inserted at the center of the trapping electrode with potential V_t. This requires the split-

TABLE I. For given electron distances d, we indicate the actual values of the geometrical parameters of the trapping device used in our simulations to obtain the results shown in Table II.

d (μm)	r_0/d	α	$\Delta z_c/\Delta z$	$\Delta z_d/\Delta z$
500	0.4	1.5	0.09	0.1
50	0.35	1.5	0.18	0.1
1.5–3	0.2	2.3	0.3	0.1

ting of each positive trapping electrode into two parts of length $(\Delta z-2\Delta z_c-\Delta z_d)/2$, as shown in Fig. 3(c). The differentiation of the trap frequencies is simply obtained by applying to each detuning electrode a different potential. Thus the voltage applied to the detuning electrode relative to the jth minimum is indicated with $V_{d,j}$.

The change in the electrostatic potential of the cavity, due to the addition of the detuning electrodes, is given by the potential $V_D(r,z)$. This potential is calculated by means of Eq. (1), with all the ring electrodes at zero potential except the detuning electrodes at potentials $V_{d,j}-V_t$ [see Fig. 3(b)]. Therefore, the resulting electrostatic potential of the cavity $V(r,z)$ is the sum of three terms

$$V(r,z) = V_T(r,z) + V_C(r,z) + V_D(r,z). \tag{11}$$

Let us evaluate the effect of the detuning electrodes on the axial frequency of the trap at the jth minimum. In our design we choose a ratio $\Delta z_d/\Delta z$ of about $1/100-1/6$. To a first approximation we can neglect the effects due to the detuning electrodes centered on other minima. Hence, from Eq. (11) the coefficient of the quadrupole term in the potential around the minimum j can be written as

$$\mathcal{C}^{(2)} = \frac{V_t\overline{C}_t^{(2)}}{d^2} + \frac{(V_c - V_t)\overline{C}_c^{(2)}}{d^2} + \frac{(V_{d,j} - V_t)\overline{C}_d^{(2)}}{d^2}, \tag{12}$$

where $\overline{C}_d^{(2)}$ is a dimensionless coefficient depending on the geometrical parameters r_0/d, α, and $\Delta z_d/\Delta z$. Its dependence on the chosen minimum can be neglected for minima not too close to the trap endcaps. The value of $\overline{C}_d^{(2)}$ varies in a range of -5 to -0.1 with the smallest values obtained for the largest values of $\Delta z_d/\Delta z$ and the smallest values of r_0/d and α. If ω_z is the axial frequency at the jth minimum produced by the trapping electrodes together with the decompensating electrodes, then the change $\delta\omega_{z,j}$ in this frequency due to the insertion of the detuning electrode around this minimum is

$$\delta\omega_{z,j} \simeq \omega_z\left(\sqrt{1 + \frac{2e(V_{d,j} - V_t)\overline{C}_d^{(2)}}{m_e d^2 \omega_z^2}} - 1\right). \tag{13}$$

The application of different potentials to the detuning electrodes centered on the traps close to the minimum j produces two effects. They shift the minimum position and increase the value of the terms in the trap potential proportional to odd powers of z. With the addition of the detuning electrodes, the coefficients of the expansion (4) with i odd can be estimated at the jth minimum as

$$\mathcal{C}^{(i)} \simeq \frac{(V_{d,j-1} - V_{d,j+1})\overline{C}_{d,near}^{(i)}}{d^i}, \tag{14}$$

where $\overline{C}_{d,near}^{(i)}$ is a dimensionless coefficient depending on the geometrical parameters r_0/d, α, and $\Delta z_d/\Delta z$. This relation is obtained from Eq. (5) by considering all the ring electrodes at zero potential except the detuning electrodes at minima $j-1$ and $j+1$. Equation (14) shows that the shifts on the minima positions, given by $\mathcal{C}^{(1)}/2\mathcal{C}^{(2)}$, and the increase of the terms $\mathcal{C}^{(3)}$, $\mathcal{C}^{(5)}$, $\mathcal{C}^{(7)}$,… are proportional to the differences between the detuning potentials. However, these effects, with the typical applied voltages, are negligible.

In order to manipulate the axial dynamics of the electrons, we need to apply, separately to each trap, an oscillating electric field. This can be obtained by adding to our device a third set of electrodes. These electrodes, defined as driving electrodes, are, in the case of m minima, m ring electrodes of width Δz_r with $\Delta z_r/\Delta z$ in a range of about $1/800-1/10$. The driving electrode is inserted, for each trap, next to a decompensating electrode, as shown in Fig. 3(c). Hence, this addition requires the shortening of the positive trapping electrodes to the width $\Delta z-2\Delta z_c-\Delta z_d-\Delta z_r$. The driving electrodes are generally held at potential V_t. However, when we apply an oscillating voltage $V_r(t)$ to the jth driving electrode, the corresponding change in the potential near the jth minimum z_j is

$$V_j(t) \simeq \frac{V_r(t)\overline{C}_r^{(1)}}{d}(z - z_j), \tag{15}$$

where $\overline{C}_r^{(1)}$ is a dimensionless coefficient depending on the geometrical parameters r_0/d, α, and $\Delta z_r/\Delta z$. This additional potential corresponds to an oscillating electric field along the axial direction. The coefficient $\overline{C}_r^{(1)}$ is obtained from Eqs. (2) and (5) by considering all the ring electrodes at zero potential except the jth driving electrode at potential $V_r(t)$. We have, according to the chosen geometry, $|\overline{C}_r^{(1)}|$ in a range of $10^{-3}-0.5$. Its value becomes larger as r_0/d and α decrease and $\Delta z_r/\Delta z$ increases.

III. SINGLE-PARTICLE OPERATIONS

When the characteristic frequencies of the trapped electrons are far detuned from each other, we have, to a good approximation, no mutual interactions. Hence, in this far-off-resonance regime, the electrons behave basically as *single* particles confined to traditional Penning traps. For the moment, therefore, we briefly review the motion of an electron in a Penning trap, neglecting the possible influence of the other particles. The dynamics of the jth electron is governed by the Hamiltonian [10]

$$H_j = \frac{(\mathbf{p}_j - e\mathbf{A}_j)^2}{2m_e} + eV - \frac{ge\hbar}{4m_e}\boldsymbol{\sigma}_j \cdot \mathbf{B}, \tag{16}$$

where e, g, and $\boldsymbol{\sigma}_j \equiv (\sigma_x^{(j)}, \sigma_y^{(j)}, \sigma_z^{(j)})$ are, respectively, the electron charge, giromagnetic factor, and Pauli matrices. The vector potential is given by

$$\mathbf{A}_j = \frac{1}{2}\mathbf{B} \times \mathbf{r}_j, \tag{17}$$

with $\mathbf{B}$ being the uniform magnetic field responsible for the radial confinement of the electron. The resulting motion can be described in terms of three independent oscillators: the cyclotron, the axial, and the magnetron motion [10]. For the trap geometry under consideration, the most interesting degrees of freedom are the axial motion and, of course, the electron spin. The electron being a spin-1/2 particle, the two

TABLE II. For a given trap distance d and axial frequency $\nu_z=\omega_z/2\pi$ we give the axial frequency detuning in the nonresonant regime between neighboring electrons $\delta_d/2\pi$, the maximum axial frequency detuning in the resonant regime between neighboring electrons $\delta_r/2\pi$, the anharmonic correction $\delta_e/2\pi$ (of the same order of $\delta_m/2\pi$), the trapping potential V_t, the decompensating potential V_c, the strength of the magnetic bottle B_1, the swapping time t_{ex} (of the same order of the gate operation time for a single electron), and the estimated decoherence time τ_d at $T=80$ mK due to thermal noise in the electrode surfaces. We assume a spin frequency $\omega_s/2\pi$ of 160 GHz. The corresponding geometrical parameters of the trap are presented in Table I. The estimated error probabilities in the swapping gate and in the single electron gates are, in case *A*, smaller than 10^{-2} and, in case *B*, smaller than 10^{-4}.

	d (μm)	ν_z (MHz)	$\delta_d/2\pi$ (MHz)	$\delta_r/2\pi$ (kHz)	$\delta_e/2\pi$ (MHz)	V_t (mV)	V_c (V)	B_1 (T/μm^2)	t_{ex} (μs)	τ_d (s)
	500	3.5	1	1.5	0.3	0.05	0.15	10^{-6}	16	2100
A	50	100	24	45	9	0.5	0.15	10^{-3}	0.55	90
	1.5	22×10^3	5000	9000	1800	5	0.05	40	0.003	0.05
	500	10	2.3	0.05	0.9	0.5	5.7	5×10^{-6}	55	3500
B	50	360	70	1.4	30	5	4.6	10^{-2}	1.7	160
	3	24×10^3	5000	100	1900	25	1.1	50	0.025	0.22

possible orientations $|\downarrow\rangle$ and $|\uparrow\rangle$ of its spin in the external magnetic field represent quite naturally the logical states $|0\rangle$ and $|1\rangle$. Problems arise when we want to encode qubits in multilevel systems, like a harmonic oscillator. This is the case of the axial oscillator. However, a solution is provided by small anharmonicities that lift the degeneracy between different transitions. Hence, for the axial motion it is necessary to introduce small anharmonicities in the quadrupole field, Eq. (6). Indeed, taking into account the octupole term in the trap potential and treating it as a small perturbation, the transition frequency between adjacent axial levels of quantum numbers k and $k+1$ is given by [10]

$$\omega_z(k) \simeq \omega_z + \delta_e\left[k+1-\frac{2\omega_z(n+l+1)}{\omega_c-\omega_m}\right], \tag{18}$$

where the shift amounts to

$$\delta_e \equiv \frac{3e\mathcal{C}^{(4)}\hbar}{m_e^2\omega_z^2} \tag{19}$$

and ω_c, ω_m, n, and l are, respectively, the frequencies and excitation numbers of the cyclotron and magnetron motion.

We suppose that, as in the case of the experiments with a single electron in a Penning trap [10], the chosen values of the magnetic and electric trapping fields give the hierarchy $\omega_m \ll \omega_z \ll \omega_c$. Under this condition, if the cyclotron motion is cooled to the ground state ($n=0$) and the magnetron radius is sufficiently shrunk ($l \ll \omega_c/\omega_z$) [23], the electrostatic correction on the axial frequency depends substantially only on the axial quantum number k:

$$\omega_z(k) \simeq \omega_z + \delta_e(k+1). \tag{20}$$

As shown in Eq. (4), the coefficient $\mathcal{C}^{(4)}$ determines the size of the main correction to the quadrupole potential. Its value depends on the potential V_c of the decompensation electrodes [see Eq. (10)]. Hence, with an appropriate choice of V_c, we can make the correction δ_e larger than the frequency width of the axial transitions. This allows us to control single axial transitions by applying electromagnetic pulses with sufficiently narrow bandwidth. Typical values of the voltage V_c used in our simulations are listed in Table II.

The manipulation of the axial states is performed by means of the driving electrodes. In particular, to act on the axial motion of a specific trapped electron, we apply an oscillating potential on the closest driving electrode. Hence, we add to the voltage V_t of this electrode a component $V_r\cos(\tilde{\omega}t-\beta)$ so that the electron energy is perturbed by the term

$$ez\mathcal{C}_r^{(1)}\cos(\tilde{\omega}t-\beta) = \frac{e\mathcal{C}_r^{(1)}}{2}\sqrt{\frac{\hbar}{2m_e\omega_z}}(a_z+a_z^\dagger)[e^{i(\tilde{\omega}t-\beta)} + e^{-i(\tilde{\omega}t-\beta)}], \tag{21}$$

where we used the relation

$$z = \sqrt{\frac{\hbar}{2m_e\omega_z}}(a_z+a_z^\dagger) \tag{22}$$

and, from Eq. (15), $\mathcal{C}_r^{(1)}=V_r\overline{\mathcal{C}_r^{(1)}}/d$.

When the driving frequency $\tilde{\omega}$ is close to the axial frequency ω_z the relevant part of the Hamiltonian of the system can be written, in the interaction picture and in rotating-wave approximation, as

$$H_z \approx \hbar\frac{\Omega}{2}(a_z^\dagger e^{i\beta}+a_z e^{-i\beta}), \tag{23}$$

where $\Omega \equiv e\mathcal{C}_r^{(1)}/\sqrt{2m_e\hbar\omega_z}$. If the oscillating potential is applied for a time t and has a sufficiently narrow bandwidth centered around the value $\omega_z(k=0)=\omega_z+\delta_e$, it produces the transformations

$$|0\rangle_z \rightarrow \cos\left(\frac{\Omega t}{2}\right)|0\rangle_z - ie^{i\beta}\sin\left(\frac{\Omega t}{2}\right)|1\rangle_z, \tag{24}$$

$$|1\rangle_z \rightarrow \cos\left(\frac{\Omega t}{2}\right)|1\rangle_z - ie^{-i\beta}\sin\left(\frac{\Omega t}{2}\right)|0\rangle_z. \tag{25}$$

Hence, the driving field can be used to realize any single-qubit gate, when considering the axial states $|0\rangle_z$ and $|1\rangle_z$ as the logical states $|0\rangle$ and $|1\rangle$. We refer to the interaction produced by the Hamiltonian (23), applied for a time t, as a $p_z(\Omega t,\beta)$ pulse.

As described in [8,9], the manipulation of the electron spin is performed by applying a small transverse oscillating magnetic field resonant with the spin precession frequency $\omega_s \equiv g|e|B/(2m_e)$:

$$\mathbf{b}(t) = b[\hat{\mathbf{i}}\cos(\omega t+\theta) + \hat{\mathbf{j}}\sin(\omega t+\theta)]. \tag{26}$$

In this case the relevant part of the system Hamiltonian becomes, in the interaction picture and rotating-wave approximation,

$$H_{IP}^{(spin)} \simeq \hbar\frac{\chi}{2}(\sigma_+ e^{-i\theta} + \sigma_- e^{i\theta}), \tag{27}$$

where $\chi \equiv g|e|b/(2m_e)$ and $\sigma_\pm \equiv (\sigma_x \pm i\sigma_y)/2$. If the small magnetic field is applied for a time t, it produces a spin-state rotation

$$|\downarrow\rangle \rightarrow \cos\left(\frac{\chi t}{2}\right)|\downarrow\rangle - ie^{-i\theta}\sin\left(\frac{\chi t}{2}\right)|\uparrow\rangle, \tag{28}$$

$$|\uparrow\rangle \rightarrow \cos\left(\frac{\chi t}{2}\right)|\uparrow\rangle - ie^{i\theta}\sin\left(\frac{\chi t}{2}\right)|\downarrow\rangle. \tag{29}$$

It can be shown that with an appropriate combination of these operations, one can perform any single-qubit gate on the spin qubit. We define the interaction produced by the Hamiltonian (27), applied for a time t, as a $p_s(\chi t,\theta)$ pulse.

However, in order to perform logic operations on a system storing quantum information in both the axial motion and the electron spin, we need an interaction between these two degrees of freedom. A possible way to accomplish this task relies on the application of an inhomogeneous static magnetic field. Indeed, with an appropriate dependence on the spatial coordinates, a static magnetic field can induce shifts on the axial transition frequencies depending on the spin-cyclotron state and vice versa. The same mechanism is already used to perform the measurement of the electron state, extracting all the relevant information on the spin and cyclotron motion from the value of the axial oscillation frequency [10]. If we consider this additional static magnetic field

$$\mathbf{B_1} = B_1\left[\left(z^2 - \frac{x^2+y^2}{2}\right)\hat{\mathbf{k}} - z(x\hat{\mathbf{i}} + y\hat{\mathbf{j}})\right], \tag{30}$$

we obtain, treating it as a perturbation, the transition frequencies

$$\omega_z(n,s,k) \simeq \omega_z + \delta_e(k+1) + \delta_m\left(n + \frac{1}{2} + \frac{g}{4}s\right), \tag{31}$$

$$\omega_s(k) \simeq \omega_s + \delta_m\left(k + \frac{1}{2}\right), \tag{32}$$

where

$$\delta_m \equiv \frac{\hbar\omega_z|e|B_1}{2m_e^2\omega_c\omega_m}. \tag{33}$$

The frequency shifts δ_e and δ_m refer, respectively, to the electrostatic and magnetic corrections. In deriving the above transition frequencies we supposed that, as in the derivation of Eq. (20), $\omega_m \ll \omega_z \ll \omega_c$ and $l \ll \omega_c/\omega_z$.

Equations. (31) and (32) clearly show the dependence of the axial and spin transition frequencies on the quantum numbers describing the state of the electron. If during the computation we keep the cyclotron oscillator in its ground state and the magnetron radius sufficiently small, we can precisely address any axial transition, without populating energy levels outside the computational space. These are reasonable assumptions, since the magnetron motion can be cooled down [10] and, at the trap temperature of 80 mK, the cyclotron remains in its ground state [11].

Having several electrons, we should also be able to singly address each of them. The individual axial frequencies are made distinguishable by applying different voltages at the detuning electrodes. As far as the single addressability of the spin qubits, one can differentiate among them by inserting a small magnetic field gradient along the z axis.

We are now in the position to discuss the implementation of conditional dynamics between the spin and axial motion of the electron. Rotations of the spin state, controlled by the axial qubit, can be realized with just one pulse. Indeed, if we apply the oscillating magnetic field, Eq. (26), on resonance with the frequency $\omega_s(n=0,k=1)$, the spin state is modified only if the axial state is $|1\rangle_z$. This opens up the possibility to implement a controlled-NOT (CNOT) gate having the spin qubit as a target and the axial qubit as a control. This two-qubit operation requires the following two pulses: a $p_s(\pi,\pi/2)$ pulse on resonance with the frequency $\omega_s(n=0,k=1)$, which flips the spin only if the axial state is $|1\rangle_z$—that is,

$$|1\rangle_z|\downarrow\rangle \rightarrow -|1\rangle_z|\uparrow\rangle, \tag{34}$$

$$|1\rangle_z|\uparrow\rangle \rightarrow |1\rangle_z|\downarrow\rangle, \tag{35}$$

without affecting the other states of the computational basis. A $p_z(2\pi,\beta)$ pulse on resonance with the frequency $\omega_z(n=0,k=1,s=1)$ to correct the minus sign in Eq. (34):

$$-|1\rangle_z|\uparrow\rangle \rightarrow |1\rangle_z|\uparrow\rangle. \tag{36}$$

To implement the other CNOT gate, with the axial qubit as a target and the spin qubit as a control, we have to apply two pulses: The driving pulse $p_z(\pi,-\pi/2)$ on resonance with the frequency $\omega_z(n=0,k=0,s=1)$ which acts on the transition $|0\rangle_z \leftrightarrow |1\rangle_z$ only if the spin state is $|\uparrow\rangle$,

$$|0\rangle_z|\uparrow\rangle \rightarrow -|1\rangle_z|\uparrow\rangle, \tag{37}$$

$$|1\rangle_z|\uparrow\rangle \rightarrow |0\rangle_z|\uparrow\rangle, \tag{38}$$

and the driving pulse $p_z(2\pi,\beta)$ on resonance with the frequency $\omega_z(n=0,k=1,s=1)$ which changes only the phase factor of the state $|1\rangle_z|\uparrow\rangle$, as illustrated in Eq. (36).

Let us evaluate the minimum operation time of one- and two-qubit gates described in this section. In order to avoid degenerate transitions and have electrostatic and magnetic corrections of the same size we can choose B_1 and V_c so that $\delta_m=\delta_e/2$. The corresponding frequency resolution required in the pulse application is $\delta_e/2$. Indeed, this quantity is the difference between neighboring frequencies corresponding to specific axial and spin transitions conditioned on, respectively, spin and axial states [see Eqs. (31) and (32)]. To produce conditional dynamics between the axial and spin states we should have $\chi,\Omega \ll \delta_e/2$. Indeed, this condition makes undesired transitions highly improbable. Since the pulse duration is of the order of π/Ω and π/χ, its minimum value is inversely proportional to the frequency resolution. The fidelity of the two-qubit gates is, for $\chi,\Omega \ll \delta_e/2$, of the order of $1-(2\chi/\delta_e)^2$ for the spin transitions and of the order of $1-(2\Omega/\delta_e)^2$ for the axial transitions (see the Appendix). The maximum axial frequency shift we use to realize conditional dynamics is $5\delta_e/2$ obtained in Eq. (31) for $\omega_z(n=0,k=1,s=1)$. Hence, by choosing $5\delta_e/2 \simeq \omega_z/5$ we obtain gate operation times varying from about 100 μs to 5 ns with fidelities ranging roughly from $1-10^{-2}$ to $1-10^{-4}$. The corresponding values of b and V_r vary in a range of, respectively, $(10^{-3}-10^{-7})$ T and $(10^{-4}-10^{-7})$ V.

The schemes described so far allow to perform arbitrary one- and two-qubit gates on a single electron. However, to make the system computationally universal, we should be able to realize conditional dynamics—i.e., CNOT gates—between qubits belonging to different electrons. This task can be accomplished by considering the electrostatic interaction between neighboring electrons in the array, as we are going to explain in the next two sections.

IV. SWAPPING GATE

In this section we describe how the Coulomb interaction between neighboring trapped electrons makes it possible to realize the swapping operation on the axial qubits. By adjusting the external voltage applied to the detuning electrodes, we can put on and off resonance the axial motion of two electrons. When in resonance, the two coupled harmonic oscillators can exchange a quantum of excitation, whereas out of resonance they basically behave as independent systems.

A. Gate description

Let us consider two electrons e_1 and e_2 separated by an average distance d (see Fig. 4). By choosing the origin of our coordinates in the center of the trap confining the electron e_1, we can write the Hamiltonian of the two particles as

$$H = H_1 + H_2 + H_{int}. \tag{39}$$

In Eq. (39), H_j, with $j=1$, 2, is the single-particle Hamiltonian, Eq. (16), of the trapped electron e_j, whereas H_{int} represents the electrostatic interaction between the two electrons (we neglect the small interaction between the spin motions),

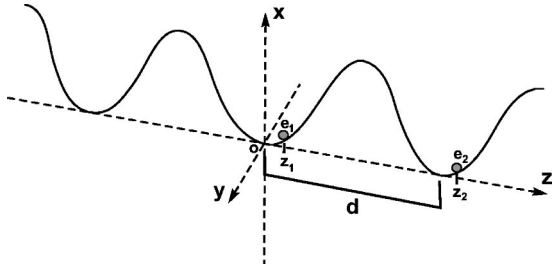

FIG. 4. Schematic drawing of two electrons e_1 and e_2 confined in neighboring microtraps separated by a distance d.

$$H_{int} = \frac{e^2}{4\pi\epsilon_0\sqrt{(x_1-x_2)^2+(y_1-y_2)^2+(z_1-z_2)^2}}, \tag{40}$$

which we can recast as

$$H_{int} = \mathcal{V}\left[1 - \frac{2[z_1-(z_2-d)]}{d} + \frac{[z_1-(z_2-d)]^2}{d^2} + \frac{(x_1-x_2)^2}{d^2} + \frac{(y_1-y_2)^2}{d^2}\right]^{-1/2}, \tag{41}$$

where $\mathcal{V}\equiv e^2/(4\pi\epsilon_0 d)$. If the oscillation amplitude of the two electrons is much smaller than the average separation d between them, we can expand the interaction Hamiltonian, Eq. (41), in a power series. To this end, we are going to evaluate the value of the displacement of the two particles with respect to the trap center. The axial displacement $|z_1-(z_2-d)|$ is of the order of the axial oscillation amplitude $\Delta z_e \equiv \sqrt{\langle z^2\rangle} \simeq \sqrt{\hbar(1+2k)/(2m_e\omega_z)}$, where k is the axial excitation number. When the two electrons are in the first excited state we obtain, in our simulations, $\Delta z_e/d$ varying from $1/325$ to $1/45$. The displacements $|x_1-x_2|$ and $|y_1-y_2|$ are of the order of the radial amplitude of the single-particle motion, $\Delta r_e \equiv \sqrt{\langle x^2\rangle} = \sqrt{\langle y^2\rangle}$. This value can be estimated by using the relations $x=\sqrt{\hbar/(2m_e\omega_c)}(a_c+a_m+a_c^\dagger+a_m^\dagger)$ and $y=i\sqrt{\hbar/(2m_e\omega_c)}(a_c-a_m-a_c^\dagger+a_m^\dagger)$ where a_c and a_m are the ladder operators of, respectively, the cyclotron and magnetron oscillators [10]. Hence we obtain $\Delta r_e \simeq \sqrt{\hbar(1+n+l)/(m_e\omega_c)}$, where n and l are, respectively, the cyclotron and magnetron quantum numbers. For the cyclotron motion in the ground state and the magnetron motion cooled to $l\simeq 10^3$ the ratio $(\Delta r_e/d)^2$ ranges, in the case of $\omega_c/2\pi \simeq 160$ GHz, from 5×10^{-7} to 5×10^{-2}. Thus, we can expand in a series H_{int} and retain terms up to the second order:

$$H_{int} \simeq \mathcal{V}\left\{\frac{1}{d}[z_1-(z_2-d)] + \frac{1}{2d^2}\{2[z_1-(z_2-d)]^2 - (x_1-x_2)^2 - (y_1-y_2)^2\}\right\}, \tag{42}$$

where we neglected the constant term $\mathcal{V}$. From the above expression, we see that in the Hamiltonian H_{int} the dynamics in the z direction is not coupled to that involving the transverse variables x and y. Then, the axial motion of the two

electrons can be studied by considering only the axial part of H:

$$H_z \simeq \frac{p_{1z}^2}{2m_e} + \frac{p_{2z}^2}{2m_e} + \frac{1}{2}m_e\tilde{\omega}_{1z}^2(z_1+d_1)^2 + \frac{1}{2}m_e\tilde{\omega}_{2z}^2(z_2-d-d_2)^2 - \frac{2\mathcal{V}}{d^2}(z_1+d_1)(z_2-d-d_2), \quad (43)$$

where we defined

$$\tilde{\omega}_{jz}^2 = \omega_{jz}^2 + \frac{2\mathcal{V}}{m_e d^2}, \quad \text{with } j=1,2, \quad (44)$$

$$d_{1,2} = d\frac{\mathcal{V}\omega_{2,1z}^2}{2\mathcal{V}(\omega_{1z}^2+\omega_{2z}^2)+m_e\omega_{1z}^2\omega_{2z}^2 d^2}. \quad (45)$$

Note that $\tilde{\omega}_{1z}$ and $\tilde{\omega}_{2z}$ are the axial frequencies of the electrons modified by the electrostatic interaction, whereas the quantities d_1 and d_2 represent the displacement of the electrons due to the Coulomb repulsion. Let us suppose that $\omega_{1z}\approx\omega_{2z}$. If we indicate with ε the ratio of the Coulomb energy, $\mathcal{V}$, to the potential energy of the second electron with respect to the first trap, $m_e\omega_{1z}^2 d^2/2$, we obtain $(\tilde{\omega}_{jz}-\omega_{jz})^2/\omega_{jz}^2 \simeq \varepsilon$ and, for $\varepsilon \ll 1$, $d_i/d \simeq \varepsilon/2$. In our simulations the quantity ε is always smaller than 10^{-2}; hence, there are very small changes both in the frequencies and trap distances.

When we introduce the ladder operators

$$\tilde{a}_{1z} = \sqrt{\frac{m_e\tilde{\omega}_{1z}}{2\hbar}}(z_1+d_1) + i\sqrt{\frac{1}{2\hbar m_e\tilde{\omega}_{1z}}}p_{1z}, \quad (46)$$

$$\tilde{a}_{2z} = \sqrt{\frac{m_e\tilde{\omega}_{2z}}{2\hbar}}(z_2-d-d_2) + i\sqrt{\frac{1}{2\hbar m_e\tilde{\omega}_{2z}}}p_{2z}, \quad (47)$$

we can recast the Hamiltonian, Eq. (43), in the form

$$H_z \simeq \hbar\tilde{\omega}_{1z}\tilde{a}_{1z}^\dagger\tilde{a}_{1z} + \hbar\tilde{\omega}_{2z}\tilde{a}_{2z}^\dagger\tilde{a}_{2z} - \frac{\hbar\mathcal{V}}{m_e d^2\sqrt{\tilde{\omega}_{1z}\tilde{\omega}_{2z}}}(\tilde{a}_{1z}+\tilde{a}_{1z}^\dagger)(\tilde{a}_{2z}+\tilde{a}_{2z}^\dagger). \quad (48)$$

From the above equation we see that the strength of the electrostatic interaction between the two particles in frequency units is given by $\xi \equiv \mathcal{V}/(m_e d^2\sqrt{\tilde{\omega}_{1z}\tilde{\omega}_{2z}})$. This quantity, if $\varepsilon \ll 1$, is much smaller than the values of the trapping frequencies—i.e., $\xi \simeq \varepsilon\omega_{1z}/2$. Thus, in this case, we can apply to the Hamiltonian (48) the rotating-wave approximation, obtaining in interaction picture, when $\omega_{1z}=\omega_{2z}$,

$$H_z^{IP} \simeq -\hbar\xi(\tilde{a}_{1z}\tilde{a}_{2z}^\dagger + \tilde{a}_{1z}^\dagger\tilde{a}_{2z}). \quad (49)$$

This is the Hamiltonian describing the electrostatic interaction between two neighboring trapped electrons with the axial frequencies tuned on resonance.

The corresponding Schrödinger equation produces, for the lower Fock states of the axial oscillators of the two particles, the temporal evolution

$$|0\rangle_{z1}|0\rangle_{z2} \to |0\rangle_{z1}|0\rangle_{z2}, \quad (50)$$

$$|0\rangle_{z1}|1\rangle_{z2} \to \cos(\xi t)|0\rangle_{z1}|1\rangle_{z2} + i\sin(\xi t)|1\rangle_{z1}|0\rangle_{z2}, \quad (51)$$

$$|1\rangle_{z1}|0\rangle_{z2} \to \cos(\xi t)|1\rangle_{z1}|0\rangle_{z2} + i\sin(\xi t)|0\rangle_{z1}|1\rangle_{z2}, \quad (52)$$

$$|1\rangle_{z1}|1\rangle_{z2} \to \cos(2\xi t)|1\rangle_{z1}|1\rangle_{z2} + \frac{i}{\sqrt{2}}\sin(2\xi t)(|0\rangle_{z1}|2\rangle_{z2} + |2\rangle_{z1}|0\rangle_{z2}). \quad (53)$$

It is easy to see that when the resonant interaction acts for a time $t_{ex} \equiv \pi/(2\xi)$, it produces, apart from phase factors, a swapping operation on the axial qubits. Indeed, it exchanges the information stored in the axial qubits of the trapped electrons. Notice that the inverse operation is realized when the resonant interaction is on for a time $3t_{ex}$. Depending on the electron distance d, we can have a swapping time t_{ex} ranging from 55 μs to 3 ns (see Table II).

The resonant interaction is switched on when the frequency detuning is much smaller than the interaction frequency—that is, $|\tilde{\omega}_{1z}-\tilde{\omega}_{2z}| \ll \xi$. On the contrary we are in the off-resonant regime when $|\tilde{\omega}_{1z}-\tilde{\omega}_{2z}| \gg \xi$. Hence, to switch on and off the resonant interaction between neighboring electrons we have to modify their axial frequencies. This is achieved by varying the voltages applied to the detuning electrodes of the two electrons, as described in Sec. II. The corresponding energy variation of the system should satisfy the following conditions: (i) it must occur in a time Δt much smaller than the swapping time t_{ex}, and (ii) it must be sufficiently slow in order to make the adiabatic theorem valid; i.e., it must occur in a time Δt such that $\Delta t \gg t_{ad}$ with $t_{ad} \equiv |\Delta E|/(\hbar\omega_z^2)$. The term ΔE represents the energy variation due to the change $\Delta\omega_z$ in the axial frequency—i.e., $\Delta E \simeq \hbar\Delta\omega_z$. Thus, the switching operation should be performed in a time window with size $t_{ex}/t_{ad} \gg 1$.

B. Gate fidelity

In our analysis of the swapping gate we made some approximations. Hence, undesired corrections may affect the dynamics of the two electrons. However, if these effects are sufficiently small, we can neglect them and efficiently perform the swapping gate. In the following we estimate the size of these undesired corrections and, at the same time, describe their dependence on the various parameters of the system. The general approach to calculate the gate fidelity and the error probability is illustrated in the Appendix. The performance of the swapping gate is mainly affected by four kinds of effects: anharmonicities in the trap potential, neglected terms in the interaction Hamiltonian, detuning and tuning accomplishment, and switching operation.

Electrostatic anharmonicities give, in Eq. (39), for the Hamiltonian of each electron, a correction term of the form

$$H_{an} \simeq e\mathcal{C}^{(3)}\left(z^3 - \frac{3}{2}zr^2\right) + e\mathcal{C}^{(4)}\left(z^4 - 3z^2r^2 + \frac{3}{8}r^4\right), \quad (54)$$

where we have set the origin of the coordinates in the trap center and considered only the main anharmonic corrections.

The rotating-wave approximation allows us to neglect the odd anharmonic correction when its strength in frequency

units, of the order of $e\mathcal{C}^{(3)}\Delta s_e^3/\hbar$ with $\Delta s_e=\max\{\Delta z_e,\Delta r_e\}$, is much smaller than the axial frequency ω_z. Indeed, in this case, if we express this correction by means of the operators a_z, a_c, and a_m we obtain, in the interaction picture, terms oscillating very rapidly and affecting the dynamics in a negligible way. This approximation gives errors, when $e\mathcal{C}^{(3)}\Delta s_e^3/\hbar \ll \omega_z$, with a probability of the order of $(e\mathcal{C}^{(3)}\Delta s_e^3/\hbar\omega_z)^2$. Differently the even anharmonic term is negligible if its size in frequency units, of the order of $e\mathcal{C}^{(4)}\Delta s_e^4/\hbar$, is much smaller than the interaction strength ξ. In this condition we have a corresponding error for this approximation, with a probability of the order of $(e\mathcal{C}^{(4)}\Delta s_e^4/\hbar\xi)^2$. According to our simulations, one can keep the probability for the above corrections sufficiently small by carefully choosing the electrode potentials.

Another source of errors for the swapping gate are the higher-order terms of the Coulomb potential expansion we neglected in Eq. (42). They produce in the interaction Hamiltonian the correction

$$H_{Coulomb} \simeq \frac{\mathcal{V}}{d^3}\left[\Delta z_{1,2}^3 - \frac{3}{2}\Delta z_{1,2}(\Delta x_{1,2}^2+\Delta y_{1,2}^2)\right] + \frac{\mathcal{V}}{d^4}\left[\Delta z_{1,2}^4 - 3\Delta z_{1,2}^2(\Delta x_{1,2}^2+\Delta y_{1,2}^2) + \frac{3}{8}(\Delta x_{1,2}^2+\Delta y_{1,2}^2)^2\right], \tag{55}$$

where $\Delta z_{1,2}\equiv z_1-(z_2-d)$, $\Delta x_{1,2}\equiv x_1-x_2$, and $\Delta y_{1,2}\equiv y_1-y_2$.

As in the case of the odd anharmonic corrections we can neglect the cubic term with the rotating-wave approximation, if its strength in frequency units, of the order of $\mathcal{V}\Delta s_e^3/\hbar d^3$, is much smaller than ω_z. In this case the error probability is of the order of $(\mathcal{V}\Delta s_e^3/\hbar d^3\omega_z)^2$. The effects due to the quartic term in Eq. (55) are negligible if its strength is small with respect to the magnitude of the quadratic term proportional to $\mathcal{V}/d^2$. In this condition the corresponding errors have a probability of the order of $(\Delta s_e/d)^4$.

We also recall that in deriving Eq. (49) we neglected, by applying the rotating-wave approximation, the terms of Eq. (48) proportional to $\tilde{a}_{1z}^\dagger\tilde{a}_{2z}^\dagger$ and $\tilde{a}_{1z}\tilde{a}_{2z}$. The errors made by this approximation have a probability, for $\xi \ll \omega_z$, of roughly $(\xi/\omega_z)^2 \simeq \varepsilon^2/4$. As shown in Table II, the probabilities of all the above errors due to the neglected terms in the Coulomb interaction can be kept, by an appropriate choice of the system parameters, sufficiently small.

The next kind of errors we analyze are those produced by the nonperfect tuning and detuning conditions. In order to evaluate them we consider the axial dynamics of the electrons when their frequencies are generally not resonant—i.e., $\omega_{2z}-\omega_{1z}=\delta$. In this case the Hamiltonian (48) can be written, in the interaction picture with respect to $\hbar\tilde{\omega}_{1z}(\tilde{a}_{1z}^\dagger\tilde{a}_{1z}+\tilde{a}_{2z}^\dagger\tilde{a}_{2z})$,

$$H_{z,d}^{IP} \simeq \hbar\delta\tilde{a}_{2z}^\dagger\tilde{a}_{2z} - \hbar\xi(\tilde{a}_{1z}\tilde{a}_{2z}^\dagger + \tilde{a}_{1z}^\dagger\tilde{a}_{2z}). \tag{56}$$

The corresponding Schrödinger equation produces, for the first Fock states of the axial oscillators, the dynamics

$$|0\rangle_{z1}|0\rangle_{z2} \to |0\rangle_{z1}|0\rangle_{z2}, \tag{57}$$

$$|0\rangle_{z1}|1\rangle_{z2} \to e^{-i(\delta t/2)}\left[\cos(\Xi t) - i\frac{\delta\sin(\Xi t)}{2\Xi}\right]|0\rangle_{z1}|1\rangle_{z2} + ie^{-i(\delta t/2)}\frac{\xi\sin(\Xi t)}{\Xi}|1\rangle_{z1}|0\rangle_{z2}, \tag{58}$$

$$|1\rangle_{z1}|0\rangle_{z2} \to e^{-i(\delta t/2)}\left[\cos(\Xi t) + i\frac{\delta\sin(\Xi t)}{2\Xi}\right]|1\rangle_{z1}|0\rangle_{z2} + ie^{-i(\delta t/2)}\frac{\xi\sin(\Xi t)}{\Xi}|0\rangle_{z1}|1\rangle_{z2}, \tag{59}$$

$$|1\rangle_{z1}|1\rangle_{z2} \to \frac{e^{-i\delta t}}{4\Xi^2}[\delta^2+4\xi^2\cos(2\Xi t)]|1\rangle_{z1}|1\rangle_{z2} - \frac{\sqrt{2}\xi e^{-i\delta t}}{4\Xi^2} \times[-\delta+\delta\cos(2\Xi t)-2i\Xi\sin(2\Xi t)]|0\rangle_{z1}|2\rangle_{z2} - \frac{\sqrt{2}\xi e^{-i\delta t}}{4\Xi^2}[\delta-\delta\cos(2\Xi t)-2i\Xi\sin(2\Xi t)] \times|2\rangle_{z1}|0\rangle_{z2}, \tag{60}$$

where $\Xi\equiv\sqrt{\xi^2+\delta^2/4}$. In the resonance condition—i.e., when $\delta\ll\xi$—the above dynamics reduces, apart from phase factors of the order of $\delta t/2$, to that described by Eqs. (50)–(53). On the contrary, when $\delta\gg\xi$, Eqs. (57)–(60) give substantially the identity transformation apart from global phase factors.

From the above relations we can estimate the fidelity of the swapping gate by considering nonperfect tuning and detuning conditions. The fidelity is defined as $|\langle\Psi_s(t)|\Psi(t)\rangle|^2$ where $|\Psi_s(t)\rangle$ is the state obtained with the ideal swapping gate and $|\Psi(t)\rangle$ is the state obtained from Eqs. (57)–(60) for finite values of δ. Hence, if we indicate by δ_r and δ_d the detuning, respectively, in and out of resonance, we have, when $\delta_r\ll\xi$ and $\delta_d\gg\xi$, a fidelity for the swapping gate of about $1-(\delta_r/\xi)^2-(\xi/\delta_d)^2$.

The change in the axial frequencies of the particles we make to switch on and off the resonant interaction should have, as described before, the following properties. It should be slow enough to occur adiabatically with respect to the single-oscillator dynamics and, at the same time, it should be quick if compared to the typical time of the resonant dynamics. Hence to obtain the swapping gate we made both the adiabatic and sudden approximation. This approximation requires that the time interval of the frequency change Δt satisfy the condition $t_{ad}\ll\Delta t\ll t_{ex}$. In this case the fidelity of the swapping gate, taking into account the corrections due to the above approximations, can be estimated as follows. The probability of undesired transitions during the adiabatic evolution is, when $\Delta t\gg t_{ad}$, of the order of $(t_{ad}/\Delta t)^2$ (see [24]). Differently undesired transitions in the sudden transformation occur, when $\Delta t\ll t_{ex}$, with a probability of the order of $(\Delta t/t_{ex})^2$. Hence we have a fidelity of the order of $1-(\Delta t/t_{ex})^2-(t_{ad}/\Delta t)^2$.

V. TWO-PARTICLE OPERATIONS

To implement the CNOT gate between the qubits of different electrons, we rely on the swapping operation described in the previous section.

Let us consider, first, the case of two neighboring electrons e_1 and e_2. To perform the CNOT gate having the spin of the first electron as a target and the axial qubit of the second one as a control, we follow this procedure: (i) We swap the information between the axial qubits; (ii) we perform the CNOT operation between the spin and the axial qubits of the same particle, according to the prescription given in Sec. III; and (iii) we swap back the information contained in the axial qubits. It is straightforward to verify that the above sequence of operations produces the desired gate.

The implementation of the CNOT gate between the axial qubits is, instead, realized as follows: (i) We swap the information between spin and axial qubits of the same electron by means of an appropriate sequence of pulses [25]; (ii) we perform the CNOT operation having the spin qubit as a target and the axial qubit as a control by applying the sequence described before; and (iii) we swap the information between the spin and axial qubits again.

We now consider the CNOT gate having the spin qubit as a control and the axial qubit as a target. This gate can be achieved with the following operations: (i) We swap the information between the spin and the axial qubits of both electrons; (ii) we perform the CNOT operation having the axial qubit as a control and the spin qubit as a target (see above); and (iii) we apply a swapping gate between the spin and axial qubits of each electron.

The implementation of the CNOT gate between the spin qubits is realized with the following steps: (i) We swap the information between the spin and the axial qubit of one electron; (ii) we perform the CNOT operation having the axial qubit as a control and the spin qubit as a target (see above); and (iii) we swap back the information between the spin and axial qubits.

Let us now generalize the procedure to electrons that are not necessarily first neighbors. For example, the CNOT gate involving the axial qubit of the nth electron as a control and the spin qubit of the first one as a target is obtained as follows: (i) We write the information, stored in the axial qubit of the nth electron onto the same qubit of the second electrons, by means of a sequence of $n-2$ swapping operations between neighboring electrons; (ii) we perform the CNOT operation between the axial qubit of the second electron and the spin of the first one, according to the prescription explained before; and (iii) we apply once again the sequence of $n-2$ swapping gates to bring back the information to the nth electron of the array. Obviously the same strategy can be extended to any other two-qubit gate between any pair of particles in the array. Hence, we are able to perform any CNOT operation between qubits of different electrons. Notice that the number of swapping operations required to implement the CNOT gate between the electrons e_1 and e_n grows linearly with n. Thus the average number of pulses, required to perform a CNOT gate, grows linearly with the number of trapped electrons—i.e., with the number of qubits in the network. Therefore, an efficient quantum algorithm, if implemented with this quantum processor, preserves its efficiency.

VI. QUBIT READOUT

In order to measure the final qubit state of our quantum processor we have to detect the axial and spin states of each trapped particle. We recall that, in the experiments with a single electron in a Penning trap, the spin-cyclotron state is routinely measured by applying a magnetic field similar to that of Eq. (30), also called a magnetic bottle, and then detecting the shift produced by this field on the axial frequency [10]. A similar technique should permit to measure the spin-cyclotron states of the trapped electrons in our system. As in the case of a single Penning trap we couple the cylindrical cavity to an external circuit. The oscillating electrons confined in the linear array of traps induce alternate image charges in the cavity electrodes, which in turn cause a current to flow through the circuit. The frequency spectrum of this current presents maxima centered at values corresponding to the axial frequencies of the trapped electrons. If we apply to each microtrap a magnetic bottle, we obtain a shift of the axial frequency of each electron depending on its cyclotron and spin quantum numbers. Hence, by measuring these shifts we can detect the spin-cyclotron state of each trapped electron.

However, in our system we need to measure the spin-axial states of the particles. This can be accomplished by applying appropriate electromagnetic pulses and then measuring the spin-cyclotron states. Let us consider a single electron. The magnetic bottle produces a shift on its cyclotron frequency depending on the axial quantum number. Its value, obtained by treating the magnetic bottle field as a small perturbation, is $\delta_m(k+1/2)$ with δ_m proportional to the magnitude of the magnetic bottle according to Eq. (33). As described in [8,9] a linearly polarized electromagnetic field can induce transitions between cyclotron energy levels. If this field is applied for an appropriate time interval with a frequency close to $\omega_c+3\delta_m/2$, it produces the transformation $|0\rangle_c \leftrightarrow |1\rangle_c$ (apart from a phase factor) only if the axial state is $|1\rangle_z$. By assuming that the cyclotron motion is initially in the ground state, we can use this pulse to substantially "copy" the information of the axial qubit to the cyclotron qubit. Hence, to perform the qubit readout we just have to apply the above field and then detect the spin-cyclotron state of the electron by remembering that the cyclotron state $|0\rangle_c(|1\rangle_c)$ corresponds to the axial state $|0\rangle_z(|1\rangle_z)$.

Let us consider the spin-cyclotron state detection. The magnetic bottle produces a shift, Eq. (31), on the axial frequency given by $\delta_m(n+1/2+gs/4)$. Unfortunately, because of the smallness of the electron anomaly, to our knowledge it is not yet possible to resolve between the shifts produced by the states: $|1\rangle_c|\downarrow\rangle$ and $|0\rangle_c|\uparrow\rangle$. To circumvent this problem we can adopt different strategies. For example, we can detect, through a quantum-nondemolition observation [11], the eventual quantum jumps to the cyclotron ground state $|0\rangle_c$. Indeed, the spin state is substantially stable while the cyclotron motion relaxes after few seconds to its ground state [10]. Another method relies on the application, after detecting the frequency shift, of a $p_s(\pi,\pi/2)$ pulse which flips the spin state. In this case the spin-cyclotron state can be detected with a second axial frequency measurement. If the frequency shift detected by this second measurement increases (decreases) of a quantity δ_m with respect to its previous value, then the spin state was initially in the state "down" ("up").

If no error occurred during the quantum computation, we should detect, for each electron, one of the spin-cyclotron

states $|0\rangle_c|\downarrow\rangle$, $|0\rangle_c|\uparrow\rangle$, $|1\rangle_c|\downarrow\rangle$, and $|1\rangle_c|\uparrow\rangle$. Hence, another method relies on the application of an appropriate sequence of electromagnetic pulses producing the transformation $|1\rangle_c \rightarrow |2\rangle_c$. This can be achieved by taking advantage of the relativistic corrections on the cyclotron frequency as indicated in [8,9]. At this point the four spin-cyclotron states are mapped onto, respectively, the states: $|0\rangle_c|\downarrow\rangle$, $|0\rangle_c|\uparrow\rangle$, $|2\rangle_c|\downarrow\rangle$, and $|2\rangle_c|\uparrow\rangle$. It is easy to verify that these states correspond to distinguishable axial frequency shifts.

In this section we have carefully analysed the qubit detection by means of axial frequency measurements. Moreover, to perform the qubit readout we can also apply capacity and charge measurement devices as in semiconductor quantum dots [19].

VII. DECOHERENCE SOURCES

In this section we analyze qualitatively and quantitatively the main decoherence mechanisms which, in principle, can affect the performances of our quantum processing device. We distinguish two main decoherence sources: thermal noise in the electrode surfaces and voltage fluctuations induced by the electronic apparatus controlling the gate dynamics. Thermal noise in the electrode surfaces is a fundamental phenomenon, in principle not eliminable and depending, for a given electrode arrangement, only on the temperature of the trapping device. Differently the noise fed into the system by the electronic apparatus depends on the properties of its electronic components, their temperature, and the characteristics of any noise reduction device. Therefore, this noise source can be, in principle, reduced, though it is difficult to estimate the ultimate technological limit. This decoherence source need to be considered since the computation in our device is performed by continuosly changing the electrode voltages. Hence, the electronic apparatus controlling these switching operations can introduce additional noise in the electrode voltages.

Thermal noise in the electrode surfaces produces fluctuating electric and magnetic fields at the position of the trapped electrons. These fluctuating fields, in turn, induce decoherence and heating in the energy eigenstates of the axial and spin electron motion. The effects on the axial motion can be analyzed with the following model [26,27]. The Hamiltonian for an electron trapped in a harmonic well subject to a fluctuating, uniform (nongradient) electric field $\mathcal{E}(t)$ is

$$H_z(t) = \frac{p_z^2}{2m_e} + \frac{1}{2}m_e\omega_z^2 z^2 + e\mathcal{E}(t)z. \tag{61}$$

By defining the ladder operator $a_z \equiv \sqrt{m_e\omega_z/(2\hbar)}z + i\sqrt{1/(2\hbar m_e\omega_z)}p_z$ we can write

$$H_z(t) = \hbar\omega_z a_z^\dagger a_z + e\mathcal{E}(t)\sqrt{\frac{\hbar}{2m_e\omega_z}}(a_z + a_z^\dagger). \tag{62}$$

From second-order perturbation theory we derive a master equation for the reduced density operator ρ_z of the axial electron motion [29]. This equation, describing the dynamics when the fluctuations of the electric field $\mathcal{E}(t)$ are traced over, can be written as

$$\dot{\rho}_z = -\frac{\gamma_+}{2}(a_z^\dagger a_z\rho_z + \rho_z a_z^\dagger a_z - 2a_z\rho_z a_z^\dagger) - \frac{\gamma_-}{2}(a_z a_z^\dagger\rho_z + \rho_z a_z a_z^\dagger - 2a_z^\dagger\rho_z a_z), \tag{63}$$

where $\gamma_\pm \equiv e^2 S_{\mathcal{E}}(\pm\omega_z)/(2\hbar m_e\omega_z)$ and $S_{\mathcal{E}}(\omega) = \int_{-\infty}^{+\infty} d\tau e^{i\omega\tau}\langle\mathcal{E}(t+\tau)\mathcal{E}(t)\rangle$ is the spectral density of the electric-field fluctuations at the electron position. From the above master equation we obtain the rates of the transitions between axial states. Indeed, if we define the quantities $\rho_{zij} \equiv {}_z\langle i|\rho_z|j\rangle_z$, we have

$$\dot{\rho}_{z00} = -\gamma_-\rho_{z00} + \gamma_+\rho_{z11}, \tag{64}$$

$$\dot{\rho}_{z01} = -\frac{3\gamma_- + \gamma_+}{2}\rho_{z01} + \sqrt{2}\gamma_+\rho_{z12}. \tag{65}$$

Equation (64) shows that the transition $|0\rangle_z \rightarrow |1\rangle_z$ ($|1\rangle_z \rightarrow |0\rangle_z$) occurs with a rate $\gamma_-(\gamma_+)$, whereas Eq. (65) gives the decay rate of the coherences between the lowest trap levels. Its value is similar to that of the level transition rates.

Hence, changes in the first Fock-state population and decoherence processes take place in a time τ_{dz} of the order of $1/\max[\gamma_-, \gamma_+, (3\gamma_- + \gamma_+)/2]$.

The spectral density $S_{\mathcal{E}}(\pm\omega_z)$ can be estimated by using the microscopic model described in [26,27]. Though this analysis considers a simple geometry of an infinite plane electrode, its results allow us to roughly evaluate τ_{zd} in our system. From this model we have

$$S_{\mathcal{E}}(\omega) \simeq \left[\frac{\hbar\omega^3}{3\pi\varepsilon_0 c^3(1 - e^{-\hbar\omega/k_B T})}\right] \times \left[2 + \frac{3\delta_s^2}{8\hat{k}d_e^3}\sqrt{\frac{1}{2} + \sqrt{\frac{1}{4} + \frac{d_e^4}{\delta_s^4}}}\right], \tag{66}$$

where $\hat{k} \equiv |\omega|/c$, $\delta_s \equiv \sqrt{(2c^2\varepsilon_0\varrho)/|\omega|}$ is the skin depth of an electrode with resistivity ϱ and d_e is the distance between electron and electrode surface.

The above relation gives the spectral density of the electric-field fluctuations in the "quasistatic" limit, where $\hat{k}d_e \ll 1$ and when the resistivity is sufficiently small so that $\hat{k}\delta_s \ll 1$. Both these conditions are verified in our system if we consider copper electrodes at $T = 80$ mK. From Eq. (66) we see that the free space spectral density, given by the blackbody field, is modified by the presence of the electrode surface. By using this equation we obtain values in our system for τ_{dz} ranging from 3500 s to 0.05 s (they coincide with the values of τ_d in Table II).

Together with a fluctuating electric field, thermal noise in the electrode surface produces a fluctuating magnetic field. This latter field induces both decoherence and heating in the spin states of the electron. The Hamiltonian for the spin motion of the trapped electron in the presence of a fluctuating magnetic field $\vec{b}(t)$ is

$$H_s(t) = \frac{\hbar}{2}\omega_s\sigma_z + \frac{ge\hbar}{4m_e}\boldsymbol{\sigma}\cdot\bar{\mathbf{b}}(t), \tag{67}$$

where ω_s is the spin precession frequency of the trapped electron. By introducing the operators $\sigma_\pm \equiv (\sigma_x \pm i\sigma_y)/2$, Eq. (67) can be rewritten as

$$H_s(t) = \frac{\hbar}{2}\omega_s(2\sigma_+\sigma_- - 1) + \frac{ge\hbar}{4m_e}[(\sigma_+ + \sigma_-)b_x(t) - i(\sigma_+ - \sigma_-)b_y(t) + (2\sigma_+\sigma_- - 1)b_z(t)]. \tag{68}$$

By using a perturbative approach we derive from the above Hamiltonian a master equation describing the dynamics of the density operator ρ_s of the electron spin motion [29]:

$$\dot{\rho}_s = -\Gamma_+(\sigma_+\sigma_-\rho_s + \rho_s\sigma_+\sigma_- - 2\sigma_-\rho_s\sigma_+) - \Gamma_-(\sigma_-\sigma_+\rho_s + \rho_s\sigma_-\sigma_+ - 2\sigma_+\rho_s\sigma_-) - 2(\Gamma_+ + \Gamma_-)((\sigma_+\sigma_-)^2\rho_s + \rho_s(\sigma_+\sigma_-)^2 - 2\sigma_+\sigma_-\rho_s\sigma_+\sigma_-), \tag{69}$$

with $\Gamma_\pm \equiv g^2e^2S_b(\pm\omega_s)/(16m_e^2)$ and where $S_b(\omega) = \int_{-\infty}^{+\infty} d\tau e^{i\omega\tau}\langle b_z(t+\tau)b_z(t)\rangle$ is the spectral density of the magnetic-field fluctuations along the z direction at the electron position. In deriving the master equation we have assumed that the noise in the components $b_x(t)$, $b_y(t)$, and $b_z(t)$ of the fluctuating field has the same strength but no correlation. From Eq. (69) we can obtain the transition and decoherence rates of the electron spin states. Indeed, by defining the matrix elements $\rho_{sij} \equiv \langle i|\rho_s|j\rangle$ with $i,j = \uparrow,\downarrow$ we have

$$\dot{\rho}_{s\downarrow\downarrow} = -2\Gamma_-\rho_{s\downarrow\downarrow} + 2\Gamma_+\rho_{s\uparrow\uparrow}, \tag{70}$$

$$\dot{\rho}_{s\downarrow\uparrow} = -3(\Gamma_- + \Gamma_+)\rho_{s\downarrow\uparrow}. \tag{71}$$

From Eqs. (70) and (71) we see that the transition $|\downarrow\rangle \rightarrow |\uparrow\rangle$ ($|\uparrow\rangle \rightarrow |\downarrow\rangle$) occurs with a rate $2\Gamma_-(2\Gamma_+)$ and the coherences $\rho_{s\downarrow\uparrow}$ decay with a rate $3(\Gamma_- + \Gamma_+)$. Hence, these processes take place in a time not smaller than $\tau_{ds} \simeq 1/[3(\Gamma_- + \Gamma_+)]$.

As in the case of the fluctuating electric field the spectral density of the fluctuating magnetic field for the simple geometry of an infinite plane electrode can be analytically calculated [27]. From this calculation we obtain, when the wavelength associated with the spin transition frequency ω_s is much larger than the distance between the electrons and trap electrodes,

$$\Gamma_\mp \simeq \pm\left[\frac{g^2e^2\hbar\omega_s^3}{48\pi\varepsilon_0 m_e^2c^5(1 - e^{\mp\hbar\omega_s/k_BT})}\right] \times\left[1 + \frac{3}{8\hat{k}_s^3\delta_s^2 d_e}\left(1 + \frac{2d_e^3}{3\delta_s^3}\right)^{-1}\right], \tag{72}$$

where $\hat{k}_s \equiv |\omega_s|/c$.

By using the above relation to estimate the decoherence time τ_{ds} for the electron in our system, we obtain values ranging from 5×10^7 s to 8 s. These values are always much larger than the corresponding values of τ_{dz}. Hence, in our device, the decoherence effects due to thermal noise in the electrode surface affect much more quickly the axial qubit than the spin qubit. If, in our processing device, thermal noise in the electrode surfaces is the main source of decoherence, then we can perform roughly 10^7–10^8 coherent operations (see Table II). However, the effects of the additional noise produced by the electronic apparatus controlling the gate switching can also be important. We estimate them with the following analysis.

Generally noise in the electrode voltage induces fluctuations, at the electron position, both in the electric field and in the electric-field gradient. Heating and decoherence of the electron axial states due to the electric-field noise induced by the electronic apparatus take place in a time τ_{dz}^{el} of the order of $2m_e\hbar\omega_z/[e^2S_{\mathcal{E}}^{el}(\omega_z)]$, where $S_{\mathcal{E}}^{el}(\omega)$ is the spectral density of the electric-field noise produced by the electronic apparatus. We suppose that this noise affects only the voltage of the detuning, driving, and decompensating electrodes. Indeed, the potential applied to these electrodes needs to be continuosly changed in a controlled manner in order to perform the quantum processing operations. We also suppose that each detuning electrode, each driving electrode, and the decompensating electrodes are affected by independent noise sources having the same strength.

The electric-field fluctuations $\delta E_j(t)$ on the electron in the jth trap depend mainly on the potential fluctuations of the nearby detuning and driving electrodes so that

$$\delta E_j(t) \simeq \frac{1}{d}\sum_{i=j-1}^{j+1}[\tilde{c}_{d,i}\delta V_{d,i}(t) + \tilde{c}_{r,i}\delta V_{r,i}(t)], \tag{73}$$

where $\delta V_{d,i}(t)$ and $\delta V_{r,i}(t)$ indicate the potential fluctuations, respectively, on the detuning and driving electrodes at the ith trap and the geometric coefficients $\tilde{c}_{d,i}$, $\tilde{c}_{r,i}$ can be calculated by using Eq. (5). From the above relation we obtain the noise spectral density

$$S_{\mathcal{E}}^{el}(\omega) \simeq \frac{S_{\mathcal{V}}^{el}(\omega)}{2d^2}\sum_{i=j-1}^{i=j+1}(|\tilde{c}_{d,i}|^2 + |\tilde{c}_{r,i}|^2), \tag{74}$$

where $S_{\mathcal{V}}^{el}(\omega)$ is the spectral density of the differential potential noise produced by the electronic apparatus.

Good room-temperature electronics have typically $S_{\mathcal{V}}^{el}(\omega_z)$ of the order of 10^{-18} V^2/Hz. However, low-temperature electronics could have $S_{\mathcal{V}}^{el}(\omega_z) \approx 10^{-21}$ V^2/Hz [16], giving values for τ_{dz}^{el} corresponding to a capability for our system of 10^4–10^6 coherent operations. These estimates are obtained by considering the geometries of Table I with the following choices: $\Delta z_d/\Delta z$ ranging from 1/10 to 1/100 and $\Delta z_r/\Delta z$ in a range of 1/80–1/800, 1/30–1/300, and 1/10–1/150 for d, respectively, equal to 500 μs, 50 μs, and 1.5–3 μs.

The electric-field gradient noise induced by the electronic apparatus produces fluctuations in the effective spring constant of the electron trap. Its effects can be estimated as follows. The Hamiltonian of an electron confined in a trap having a spring constant with a fluctuation $\tilde{\epsilon}(t)$ is

$$H_z(t) = \frac{p_z^2}{2m_e} + \frac{1}{2}m_e\omega_z^2[1 + \tilde{\epsilon}(t)]z^2, \tag{75}$$

which can be rewritten as

$$H_z(t) = \hbar\omega_z a_z^\dagger a_z + \frac{\hbar\omega_z\tilde{\epsilon}(t)}{4}(a_z^{\dagger 2} + a_z^2 + 2a_z^\dagger a_z + 1). \quad (76)$$

This noise induces both decoherence in the superpositions of the first Fock axial states and heating with transitions $|0\rangle_z \rightarrow |2\rangle_z$. The heating rate $R_{0\rightarrow 2}$ can be estimated by using the first-order time-dependent pertubation theory [28]

$$R_{0\rightarrow 2} \simeq \left(\frac{m_e\omega_z^2}{2\hbar}\right)\int_{-\infty}^{+\infty} d\tau e^{2i\omega_z\tau}\langle\tilde{\epsilon}(t)\tilde{\epsilon}(t+\tau)\rangle\big|_z\langle 0|z^2|2\rangle_z|^2$$

$$= \frac{\omega_z^2}{8}S_{\tilde{\epsilon}}(2\omega_z), \quad (77)$$

where $S_{\tilde{\epsilon}}(\omega) \equiv \int_{-\infty}^{+\infty} d\tau e^{i\omega\tau}\langle\tilde{\epsilon}(t)\tilde{\epsilon}(t+\tau)\rangle$ is the spectral density of the noise $\tilde{\epsilon}(t)$.

The rate of decoherence in the first Fock state superposition can be estimated by considering in Eq. (76) only the effect due to the term proportional to $\tilde{\epsilon}(t)a_z^\dagger a_z$. The corresponding master equation, obtained by using a perturbative approach, for the density operator ρ_z describing the axial electron motion is [29]

$$\dot{\rho}_z = -\frac{S_{\tilde{\epsilon}}(\omega_z)\omega_z^2}{8}[(a_z^\dagger a_z)^2\rho_z + \rho_z(a_z^\dagger a_z)^2 - 2a_z^\dagger a_z\rho_z a_z^\dagger a_z]. \quad (78)$$

From the above equation we can derive the equation for the coherence ρ_{z01}:

$$\dot{\rho}_{z01} = -\frac{S_{\tilde{\epsilon}}(\omega_z)\omega_z^2}{8}\rho_{z01}. \quad (79)$$

We suppose that the noise spectrum has the same strength at frequencies $2\omega_z$ and ω_z. Consequently the effects of heating and decoherence due to the noise in the spring constant of the electron trap occur roughly at the same rate.

By assuming that in our system the noise produced by the electronic apparatus does not affect the trapping electrodes we have

$$\frac{1}{2}m_e\omega_z^2\tilde{\epsilon}(t) \simeq \frac{e}{d^2}[\overline{C}_c^{(2)}\delta V_c^{el}(t) + \overline{C}_d^{(2)}\delta V_d^{el}(t)], \quad (80)$$

where $\delta V_c^{el}(t)$ and $\delta V_d^{el}(t)$ are the potential fluctuations produced by the electronic apparatus on, respectively, the compensating and detuning electrodes of the specific electron trap.

If we consider these two voltage noise sources independent and having the same strength, we obtain, from the above relation,

$$S_{\tilde{\epsilon}}(\omega) \simeq \frac{2e^2}{m_e^2\omega_z^4 d^4}S_V^{el}(\omega)[|\overline{C}_c^{(2)}|^2 + |\overline{C}_d^{(2)}|^2]. \quad (81)$$

An estimate of the decoherence and heating time due to electric field gradient noise, given by $1/R_{0\rightarrow 2}$, can be obtained from Eq. (77) by using the above relation. Its value in our system, if we consider $S_V^{el}(\omega) \approx 10^{-21}\ V^2/\mathrm{Hz}$, is always larger or of the same order of the decoherence time τ_{dz}^{el} due to the electric field noise.

Hence, with voltage fluctuations of the electronic apparatus of the order of 3×10^{-2} nV, our processing device can perform 10^4–10^6 coherent operations. This corresponds to an error probability per gate below the threshold for fault-tolerant computation. Moreover, since the fundamental upper limit of the decoherence time depends only on thermal noise, the number of coherent operations can be, in principle, further increased.

VIII. CONCLUSION

In this paper we have shown that a system consisting of trapped electrons in vacuum can be a valid candidate for a scalable quantum computer. This arrangement presents three major advantages: high clock speed, low decoherence, and scalability. In particular, in our design several electrons are confined in a linear array of Penning trap by means of an innovative trapping device. Quantum information is encoded in the axial and spin motion of each single particle. Universal computation is performed by applying electromagnetic pulses in combination with static fields and by controlling the Coulomb interaction between neighboring electrons. The qubit readout can be achieved by axial frequency measurements as in traditional Penning traps or by capacitance and charge measurements as in semiconductor quantum dots.

The results of an in-depth analysis of the main error and decoherence sources demonstrate that the system permits fault-tolerant computation (error probabilities per gate of about 10^{-6}–10^{-4}) within current experimental capabilities. A fundamental requirement of our scheme is the ground-state cooling of the axial motion. Though not yet experimentally demonstrated, this task should be, by applying specific techniques [10,12,30], within the reach of present technology. Furthermore, at temperatures of tens of mK, for interelectron distances smaller than 20 μm and axial trapping frequencies in the GHz range, thermalization with the trap environment brings the axial oscillator to its ground state without any external cooling.

Our current and future work on the system will mainly concern two areas of research. First, we should further analyze and improve the qubit detection technique. For example, the time required to measure the axial frequency in experiments with a single electron [11] is not fast when compared to the estimated decoherence times. We recall that though fast measurement capability is not an essential prerequisite for quantum error correction, it reduces the number of required gate operations [31]. Furthermore, detection techniques based on charge and capacitance measurements as in semiconductor quantum dots should be also applicable to our system. They could improve the detection capabilities in terms of efficiency and speed.

The other direction of our future research work will concern the possibility to increase the clock speed of the system in order to perform a larger number of gate operations within the decoherence time. The clock frequency of our current scheme is limited by the strength of the frequency corrections produced by static inhomogeneous fields—i.e., anharmonic electrostatic field and magnetic bottle. These corrections are much smaller than the axial frequencies. Therefore,

the potentiality related to the high trapping frequencies of the electrons is not fully exploited. A possible scheme, able to avoid the use of the anharmonic corrections and then increase the clock speed, could exploit the technique of composite pulses already used in NMR [32] and ion-trap systems [5].

ACKNOWLEDGMENTS

This research has been carried out within the framework of Contract No. PAIS-MEPTRAP, funded by INFM, and by the European Union under Contract No. IST-FP6-003772 (QUELE).

APPENDIX

In this appendix we describe how to estimate the fidelity and error probability of the gate operations, when we include corrective effects neglected in the limit of the approximations made to obtain the "ideal" dynamics shown in the paper.

In particular, the transformations realizing single-qubit and two-qubit operations on a single electron are obtained by making the following approximations. We neglect in the interaction Hamiltonian terms which oscillate very rapidly (rotating-wave approximation) and do not consider the possibility to leave the computational space. Moreover, the resonant dynamics producing the swapping gate is obtained by neglecting anharmonic corrections in the electron trapping potential, higher-order terms in the Coulomb energy, and effects due to the change in the axial frequency.

In general the real dynamical evolution of the system, during gate operations, is different from the "ideal" dynamics obtained with the above approximations. Consequently deviations from the ideal dynamics can lead to errors in the gate operations.

Let us suppose that the global Hamiltonian of the system can be written as

$$H(t) = H_0 + H'(t), \tag{A1}$$

where H_0 is time independent and $H'(t)$ is the Hamiltonian, in general time dependent, of the interaction producing the specific gate operation. The state vector $|\Psi(t)\rangle$ of the system satisfies the Schrödinger equation

$$i\hbar \frac{\partial |\Psi(t)\rangle}{\partial t} = H(t)|\Psi(t)\rangle. \tag{A2}$$

If we indicate by $E_k^{(0)}$ and $|\Psi_k^{(0)}\rangle$, respectively, the eigenvalues and orthonormal eigen-vectors of the unperturbed Hamiltonian H_0, we can write

$$|\Psi(t)\rangle = \sum_k c_k(t)|\Psi_k^{(0)}\rangle e^{-iE_k^{(0)}t/\hbar}, \tag{A3}$$

where $|c_k(t)|^2 = |\langle \Psi_k^{(0)}|\Psi(t)\rangle|^2$ is the probability of finding the system in the state $|\Psi_k^{(0)}\rangle$.

By substituting the expansion (A3) into the Schrödinger equation (A2) and then taking the scalar product with a vector $|\Psi_b^{(0)}\rangle$ we find

$$\dot{c}_b(t) = \frac{1}{i\hbar}\sum_k H'_{bk}(t)c_k(t)e^{i\omega_{bk}t}, \tag{A4}$$

where $H'_{bk}(t) = \langle \Psi_b^{(0)}|H'(t)|\Psi_k^{(0)}\rangle$ and $\omega_{bk} = (E_b^{(0)} - E_k^{(0)})/\hbar$.

The set of equations (A4) for all b constitues a system of first-order coupled differential equations strictly equivalent to the Schrödinger equation (A2).

In order to estimate the errors due to the specific approximations made in the interaction dynamics we proceed as follows. We insert the approximated solutions $c_k^{app}(t)$, describing the "ideal" gate dynamics shown in the paper, on the right-hand side of Eq. (A4) and integrate over time, obtaining

$$c_b^{act}(t) \simeq \frac{1}{i\hbar}\sum_k \int_{t_0}^{t} H'_{bk}(t')c_k^{app}(t')e^{i\omega_{bk}t'}dt. \tag{A5}$$

The normalized coefficient $c_b^{act}(t)/\sqrt{\Sigma_k |c_k^{act}(t)|^2}$ represents a more precise estimate of $c_b(t)$ with respect to $c_b^{app}(t)$.

The fidelity $F(t)$ of the gate operation is defined as

$$F(t) = |\langle \Psi_{app}(t)|\Psi(t)\rangle|^2, \tag{A6}$$

where $|\Psi_{app}(t)\rangle$ is the state vector of the system obtained with the approximated solutions describing the "ideal" gate dynamics and $|\Psi(t)\rangle$ is the state vector describing the actual dynamical evolution. Hence the error probability is defined as $P_e(t) = 1 - F(t)$.

In order to estimate $F(t)$ we use the relations $|\Psi_{app}(t)\rangle = \Sigma_k c_k^{app}(t)|\Psi_k^{(0)}\rangle e^{-iE_k^{(0)}t/\hbar}$ and $|\Psi(t)\rangle \simeq \Sigma_k [c_k^{act}(t)/\sqrt{\Sigma_k |c_k^{act}(t)|^2}]|\Psi_k^{(0)}\rangle e^{-iE_k^{(0)}t/\hbar}$, obtaining

$$F(t) \simeq \frac{|\sum_k c_k^{*app}(t)c_k^{act}(t)|^2}{\sum_k |c_k^{act}(t)|^2}. \tag{A7}$$

In general, in the cases considered, $F(t)$ is always, during the system evolution, not smaller than a value F_{min}. Hence in the paper we always choose as a fidelity and error probability the time-independent values, respectively, of F_{min} and $1 - F_{min}$.

[1] For a review see the Quantum Computation Roadmap at the internet site http://qist.lanl.gov.

[2] C. Monroe, D.M. Meekhof, B.E. King, W.M. Itano, and D.J. Wineland, Phys. Rev. Lett. **75**, 4714 (1995).

[3] B. DeMarco, A. Ben-Kish, D. Leibfried, V. Meyer, M. Rowe, B.M. Jelenkovic, W.M. Itano, J. Britton, C. Langer, T. Rosenband, and D.J. Wineland, Phys. Rev. Lett. **89**, 267901 (2002).

[4] D. Leibfried, B. DeMarco, V. Meyer, D. Lucas, M. Barrett, J. Britton, W.M. Itano, B. Jelenkovic, C. Langer, T. Rosenband, and D.J. Wineland, Nature (London) **422**, 412 (2003).

[5] S. Gulde, M. Riebe, G.P.T. Lancaster, C. Becher, J. Eschner, H. Häffner, F. Schmidt-Kaler, I.L. Chuang, and R. Blatt, Nature (London) **422**, 48 (2003).
[6] G. Ciaramicoli, I. Marzoli, and P. Tombesi, Phys. Rev. Lett. **91**, 017901 (2003).
[7] S. Mancini, A.M. Martins, and P. Tombesi, Phys. Rev. A **61**, 012303 (2000).
[8] G. Ciaramicoli, I. Marzoli, and P. Tombesi, Phys. Rev. A **63**, 052307 (2001).
[9] G. Ciaramicoli, I. Marzoli, and P. Tombesi, J. Mod. Opt. **49**, 1307 (2002).
[10] L.S. Brown and G. Gabrielse, Rev. Mod. Phys. **58**, 233 (1986).
[11] S. Peil and G. Gabrielse, Phys. Rev. Lett. **83**, 1287 (1999).
[12] B. D'Urso, B. Odom, and G. Gabrielse, Phys. Rev. Lett. **90**, 043001 (2003).
[13] M. Drndić, C.S. Lee, and R.M. Westervelt, Phys. Rev. B **63**, 085321 (2001).
[14] J.I. Cirac and P. Zoller, Phys. Rev. Lett. **74**, 4091 (1995).
[15] J.I. Cirac and P. Zoller, Nature (London) **404**, 579 (2000).
[16] B.E. Kane, Nature (London) **393**, 133 (1998).
[17] D. Loss and D.P. DiVincenzo, Phys. Rev. A **57**, 120 (1998).
[18] D.J. Heinzen and D.J. Wineland, Phys. Rev. A **42**, 2977 (1990).
[19] *Mesoscopic Electron Transport*, edited by L.L. Sohn, L.P. Kouwenhoven, and G. Schon (Kluwer Academic, Dordrecht, 1996).
[20] F.M. Penning, Physica (Amsterdam) **3**, 873 (1936).
[21] J.D. Jackson, *Classical Electrodynamics*, 2nd ed. (Wiley, New York, 1975).
[22] E. Durand, *Électrostatique-Problèmes Généraux Conducteurs* (Masson et Cie, Paris, 1966).
[23] In principle the selective control of single axial transitions is possible when the magnetron motion is either in a statistical mixture with quantum numbers in a range $\Delta l \ll \omega_c/\omega_z$ or in a pure Fock state. Typically the magnetron quantum number changes in a time much larger than the decoherence time of the axial motion. Hence the above conditions assure the possibility to act on specific axial transitions without populating other energy states.
[24] B.H. Bransden and C.J. Joachain, *Introduction to Quantum Mechanics* (Longman Scientific and Technical, London, 1989).
[25] This sequence consists of three CNOT gates, in which the two qubits play alternatively the role of the control and of the target.
[26] Q.A. Turchette, D. Kielpinski, B.E. King, D. Leibfried, D.M. Meekhof, C.J. Myatt, M.A. Rowe, C.A. Sackett, C.S. Wood, W.M. Itano, C. Monroe, and D.J. Wineland, Phys. Rev. A **61**, 063418 (2000).
[27] C. Henkel, S. Pötting, and M. Wilkens, Appl. Phys. B: Lasers Opt. **69**, 379 (1999).
[28] T.A. Savard, K.M. O'Hara, and J.E. Thomas, Phys. Rev. A **56**, R1095 (1997).
[29] C.W. Gardiner, *Quantum Noise* (Springer-Verlag, Berlin, 1991).
[30] G. Gabrielse and J.N. Tan, in *Cavity Quantum Electrodynamics*, edited by P. Berman (Academic Press, New York, 1994).
[31] D.P. DiVincenzo, Fortschr. Phys. **48**, 771 (2000).
[32] A.M. Childs and I.L. Chuang, Phys. Rev. A **63**, 012306 (2001).